

Electron density and temperature measurements with Thomson scattering in a hydrogen microwave plasma

M.D. Ruijzendaal¹, D. Del Cont-Bernard¹, T.W.H. Righart¹, G.J. van Rooij¹, T. Butterworth¹

¹ *Department of Circular Chemical Engineering, Maastricht University, Maastricht, The Netherlands*

Abstract: Electron temperature (T_e) and density (n_e) are targeted in hydrogen microwave plasma for understanding of power deposition and dissociation. This work reports the commissioning of Thomson scattering for this purpose. First results demonstrate the viability of the approach. Experiments in scans of power and pressure will be used to estimate the reactor performance in terms of atomic hydrogen production efficiency.

Keywords: Hydrogen plasma, Thomson scattering, electron density, electron temperature

1. Introduction

In plasma chemistry, electrons drive chemical reactions: through direct participation in reactions, collisional excitations of molecules, and as a source of heat [1]. Here, we investigate the electron density and temperature in a hydrogen plasma using Thomson scattering. We use the hydrogen plasma as a radical source to initiate chemical reactions in methane injected downstream, where it enables non-oxidative coupling to produce high value hydrocarbons: acetylene and ethylene [2, 3]. Hydrogen plasmas are also of interest for e.g. testing of fusion reactor walls [4, 5], EUV lithography machines [6] and diamond synthesis [7].

In all these applications, the characteristics of the electrons determine the resultant process. As such, it is important to have diagnostic methods to gain insight in the density and temperature of the electrons. Methods such as optical emission spectroscopy [8], Stark broadening [9], and interferometry [10] are commonly used but are indirect or spatially unresolved measurements of electron properties.

Laser scattering is the preferred direct measurement of electron temperature and density. These parameters can be derived from the way laser light scatters off electrons, which is called Thomson scattering [11]. The application of this diagnostic is limited to point measurements of scattering spectra using a spectrometer, though it can be extended to 1D and 2D by repeated measurements or using fiber arrays.

In this study, we present Thomson scattering spectroscopy performed in a microwave plasma ignited in hydrogen. The viability of the method is demonstrated here by point-measurements. We will produce 2D maps of electron temperature and density by performing radial scans with an axial fiber array. These can be used to determine reactor performance, by measures such as power density and atomic hydrogen production efficiency.

2. Diagnostic design criteria

Some plasma setups are better suited for the Thomson scattering diagnostic than others. The main criteria are briefly discussed here.

Firstly, the Thomson scattering signal might be obscured or overwhelmed by other spectral features. Rayleigh scattering and stray laser light are commonly orders of magnitude larger than the Thomson signal. Proper

exposure of a camera to the total signal means that the Thomson signal will be practically invisible. Notch filters or longpass filters are used to overcome this issue [12].

Raman scattering also commonly interferes with Thomson scattering signal but cannot be as easily blocked due to its repetitive occurrence in the region of interest. Various strategies are described to tackle this issue. Atomic gases, with a few notable exceptions [13], don't have Raman signals, making noble gases or plasmas with a high dissociation degree suitable for Thomson scattering. The same is true for gases with spherical-top symmetry, unless the plasma produces a significant amount of another species that interferes. A methane plasma is an example, where produced C_2 molecules produce a strong LIF signal that constrains the explorable parameter space [14]. As for our experiments, H_2 falls into the category of molecules that have a high separation of Raman features such that they are distant from the spectral region in which Thomson scattering is dominant [15, 16].

If the strategies above cannot completely avoid them, the interfering signals need to be carefully distinguished from the Thomson scattering signal by means of spectral synthesis [12, 17]. For illustrative purposes, a synthetic spectrum with combined signals of Thomson, Rayleigh and Raman scattering is shown in Fig. 1. The Rayleigh signal and rotational Raman of H_2 are clearly spectrally distinct from the Thomson signal, enabling a relatively easy isolation of the Thomson signal.

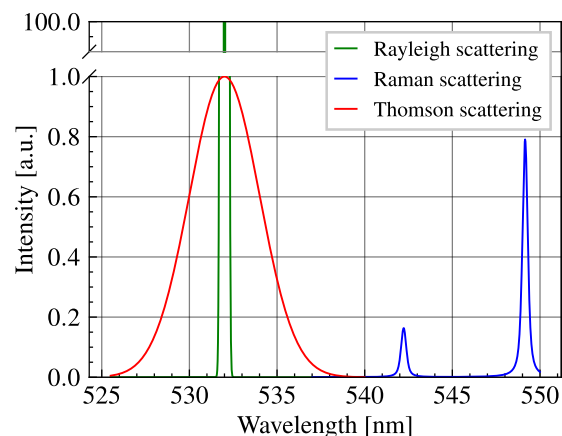


Fig. 1. Synthetic spectrum of a hydrogen plasma showing Thomson, Rayleigh, and H_2 rotational Raman scattering. The vertical axis is broken to show Rayleigh intensity.

Secondly, it is important to consider the design criteria for the spectrometer. If the bulk of the electrons have a Maxwellian energy distribution, the spectral broadening profile $f(\lambda)$ is a Gaussian function [11, 18]

$$f(\lambda) = A \exp\left(-\frac{(\lambda-\lambda_l)^2}{\Delta\lambda_{1/e}^2}\right). \quad (1)$$

The electron density n_e can be determined from the scattering amplitude A , and the electron temperature T_e can be determined from the Gaussian width $\Delta\lambda_{1/e}$ as

$$T_e = \frac{m_e c^2}{4 k_B} \cdot \left(\frac{\Delta\lambda_{1/e}}{\lambda_l}\right)^2 \quad (2)$$

where m_e, c, k_B are respectively the electron mass, speed of light, and Boltzmann constant. As a 532 nm laser is used for this work, an electron temperature of 1 or 3eV will have an intensity equal to A/e at respectively 1.5 nm and 2.6 nm from the laser wavelength. A spectral region of 526-538nm is required to fully image these Thomson spectra. It is worth considering collecting that spectral region in a narrow region on the camera sensor rather than distributing it over the complete sensor. This is a balance between an increased signal-to-noise ratio, decreased acquisition time and decreased spectral resolution.

Lastly, the signal throughput must be carefully considered. A large acceptance angle, or equivalently a low F-number or high numerical aperture, is preferred to maximize the collected signal. It must be noted that this applies to the complete set of collection optics, fiber bundles, and spectroscopy entrance slit.

3. Experimental methods

Experimental setup

We briefly describe the experimental setup used for this study, as shown in Fig. 2 [16]. Microwave (MW) radiation is generated using a 2.45GHz solid-state microwave power supply (pinkRF) and through waveguides (WR340) directed into a MW applicator. A sliding short is positioned at the end of the applicator such that a standing wave will form inside the applicator. A 30mm diameter quartz tube is positioned at the location of an anti-node (i.e., electric field maximum). The MW radiation is tuned for minimum reflectance using a 3-stub impedance autotuner (S-TEAM HOMER). With sufficient power applied, a plasma forms in the axial center of the quartz tube.

The pressure, flow and gas composition inside the quartz tube can all be regulated. For the experiments in this work, 80 mbar hydrogen gas was used at a flow rate of 20 slm. Gas flows through tangential inlets into the reactor, creating a vortex that constrains the hot plasma to the axial center of the tube (i.e., forward vortex configuration).

A 532 nm Nd:YAG laser beam (Powerlite DLS 9030, 8 ns pulses at 30 Hz, energy < 1.1 J per pulse), coincident with the tube axis, is focused using a pair of 10 cm offset perpendicular cylindrical lenses ($f = 1750$ mm) in the center of the microwave applicator and plasma core. Scattered light is collected perpendicular to the laser beam, and is collimated using a 100 mm lens, filtered using a polarizing filter and a 532 nm longpass filter (Semrock

RazorEdge – slightly rotated to blue-shift the transmission window), and then imaged onto an optical fiber array (19 fibers spanning a 6mm line) using a second 100mm lens. The fibers are mounted on the entrance slit of a spectrometer (Andor Kymera 193i) imaging onto a gated intensified CCD camera (Andor iStar 334T 18F-63).

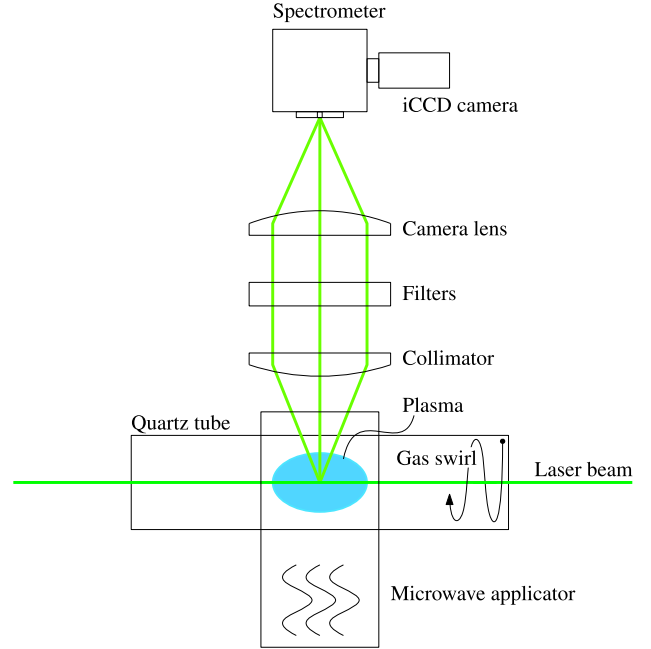


Fig. 2. Schematic drawing of the setup for plasma generation and optical diagnostics.

Procedure and data processing

The laser pulses are time-synchronized with the camera gate window to maximize the signal-to-noise ratio. A background signal (i.e. acquisition without a laser pulse) is subtracted from every measurement. Spectral regions with interfering signals (Rayleigh, Raman) and partially absorbed Thomson signal are excluded from the analysis. The remainder of the data is then fit to Eq. 1 with Eq. 2.

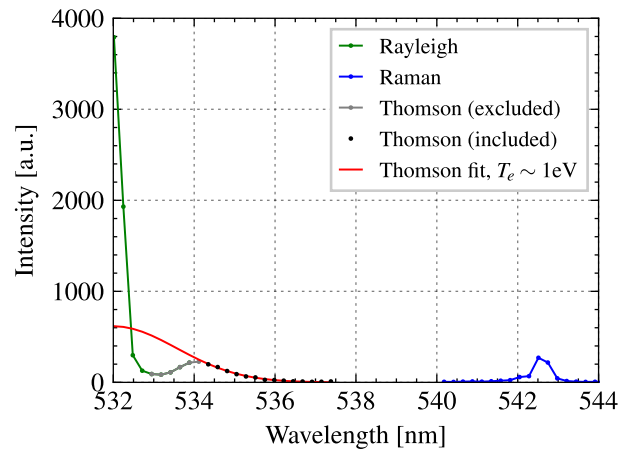


Fig. 3. Measurement of laser scattering in hydrogen plasma. Spectrum is split and labelled for clarity. Dots: data points, red line: fit to Thomson signal.

4. Results

Measurements and their analyses are in progress. An initial result is displayed in Fig. 3, showing distinct signals for Thomson, Rayleigh, and Raman scattering. Note that, even with a filter, Rayleigh scattering is still dominant over Thomson scattering. Preliminary analysis yields a fit corresponding to an electron temperature of approximately 1eV. Absolute reference signals based on Raman scattering in H₂ and N₂ are underway to determine electron densities from the intensity of Thomson scattering signal.

5. Conclusions and outlook

We have demonstrated the measurement of electron temperature and density using Thomson scattering in a pure H₂ microwave generated plasma. Electron density and temperature data will be used to determine energy transfer mechanisms in H₂ plasmas used for methane conversion. In support of this objective, we have also developed a novel technique for 2D imaging of H₂ rotational and vibrational temperatures [16]. We also plan to expand this 2D imaging technique to Thomson scattering in the near future. We envisage that these methods will be used to gain critical insight into the physics and chemistry of hydrogen containing plasmas.

6. References

- [1] A. Fridman, Cambridge University Press (2008).
- [2] K. Gehrman and H. Schmidt, Proc. – 8th World Petr. Congr. (1971).
- [3] H. Gladisch, Chem. Ing. Tech., **41**, 204 (1969).
- [4] H.J. van der Meiden, R.S. Al, C.J. Barth et al., Rev. Sci. Instrum., **79**, 013505 (2008).
- [5] J. Rapp, W.R. Koppers, H.J.N. van Eck et al., Fusion Eng. Des., **85**, 1455 (2010).
- [6] J. Beckers, T. van de Ven, R. van der Horst et al., Appl. Sci., **9**, 2827 (2019).
- [7] M. Kamo, Y. Sato, S. Matsumoto et al., J. Cryst. Growth, **62**, 642 (1983).
- [8] V.M. Donnelly, J. Phys. D: Appl. Phys., **37**(19), R217 (2004).
- [9] M.A. Gigosos, J. Phys. D: Appl. Phys., **47**, 343001 (2014).
- [10] F. Leipold, R.H. Stark, A. El-Habachi et al., J. Phys. D: Appl. Phys., **33**, 2268 (2000).
- [11] J. Sheffield, Academic Press (1975).
- [12] A.F.H. van Gessel, E.A.D. Carbone, P.J. Bruggeman et al., Plasma Sources Sci. Technol., **21**, 015003 (2012).
- [13] C.J. Dasch and J.H. Bechtel, Opt. Lett. **6**, 36 (1981).
- [14] T. Butterworth, A. van de Steeg, D. van den Bekerom et al., Plasma Sources Sci. Technol., **29**, 095007 (2020).
- [15] K.P. Huber and G. Herzberg, Van Nostrand (1979).
- [16] D. Del Cont-Bernard, M.D. Ruijzendaal, T. Righart et al., Conf. Proc. – 25th Int. Symp. Plasma Chem. (2023).
- [17] B.L.M. Klarenaar, O. Guaitella, R. Engeln et al., Plasma Sources Sci. Technol., **27**, 085004 (2018).
- [18] E. Carbone and S. Nijdam, Plasma Phys. Controlled Fusion, **57**, 014026 (2014).